Eur. Phys. J. C 23, 455–461 (2002)
Digital Object Identifier (DOI) 10.1007/s100520100835

THE EUROPEAN PHYSICAL JOURNAL C

Future measurements of deeply virtual Compton scattering

V.A. Korotkov[1,2], W.-D. Nowak[2]

[1] IHEP, 142284 Protvino, Russia
[2] DESY Zeuthen, 15738 Zeuthen, Germany

Received: 13 August 2001 / Revised version: 23 October 2001 /
Published online: 15 March 2002 –

Abstract. Prospects for future measurements of deeply virtual Compton scattering are studied in leading order using different simple models for the parameterizations of generalized parton distributions (GPDs). Measurements of the lepton charge and lepton beam helicity asymmetry will yield important input for theoretical models towards the future extraction of GPDs. The kinematics of the HERMES experiment, complemented with a recoil detector, was adopted to arrive at realistic projected statistical uncertainties.

1 Introduction

The study of hard exclusive processes in the Bjorken limit is now considered as a promising tool to gain new insight in the details of the nucleon structure that cannot be studied with inclusive deep inelastic scattering (DIS). A unified theoretical description of hard exclusive and inclusive processes has been obtained through the formalism of generalized parton distributions [1–5] (see the recent reviews in [7,8]) which are also called skewed, off-forward or non-forward parton distributions.

An ordinary parton distribution represents the probability to find a parton with a specified longitudinal momentum fraction x in the fast moving hadron and thus is summed over all partonic configurations containing such a parton. In contrast, GPDs represent the interference of two different wave functions, one with a parton having momentum fraction $x+\xi$ and another one with a parton having momentum fraction $x-\xi$. GPDs, besides the longitudinal momentum fraction variables x and ξ (called the skewedness parameter), depend on a third independent variable, the momentum transfer $\Delta^2 = (p-p')^2$ between initial and final nucleon states with momenta p and p', respectively.

There are four different types of quark GPDs contributing to the simplest hard exclusive process: deeply virtual Compton scattering (DVCS), $ep \longrightarrow ep\gamma$. The detailed form of the Compton amplitude can be found in [5]. The overall picture remains valid also in the case of additional meson production in DVCS [6]. In the unpolarized distributions, $H^q(x,\xi,\Delta^2)$ and $E^q(x,\xi,\Delta^2)$, the quark helicities are summed over. The polarized distributions, $\widetilde{H}^q(x,\xi,\Delta^2)$ and $\widetilde{E}^q(x,\xi,\Delta^2)$, are responsible for the differences between right- and left-handed quarks.

The generalized parton distributions combine the characters of both the ordinary parton distributions and of nucleon form factors. On the one hand, in the limit $\Delta^2 \to 0$, $\xi \to 0$,

$$H^q(x,0,0) = q(x), \quad \widetilde{H}^q(x,0,0) = \Delta q(x), \tag{1}$$

where $q(x)$ and $\Delta q(x)$ are the ordinary quark number density and quark helicity distributions. On the other hand, the first moment of GPDs must satisfy the following sum rules:

$$\begin{aligned}
\int_{-1}^{1} \mathrm{d}x H^q(x,\xi,\Delta^2) &= F_1^q(\Delta^2),\\
\int_{-1}^{1} \mathrm{d}x E^q(x,\xi,\Delta^2) &= F_2^q(\Delta^2),\\
\int_{-1}^{1} \mathrm{d}x \widetilde{H}^q(x,\xi,\Delta^2) &= g_A^q(\Delta^2),\\
\int_{-1}^{1} \mathrm{d}x \widetilde{E}^q(x,\xi,\Delta^2) &= h_A^q(\Delta^2),
\end{aligned} \tag{2}$$

where $F_1^q(\Delta^2)$ and $F_2^q(\Delta^2)$ are the Dirac and Pauli form factors and $g_A^q(\Delta^2)$ and $h_A^q(\Delta^2)$ are the axial-vector and pseudo-scalar form factors, respectively.

In the above formulae the variable x is defined in the range $(-1,+1)$ and negative values correspond to anti-quark distributions in the following manner:

$$q(-x) = -\bar{q}(x), \quad \Delta q(-x) = \Delta\bar{q}(x). \tag{3}$$

Two different regions exist for GPDs with respect to the variables x and ξ. For $|x| > \xi$ the GPDs are the generalizations of the ordinary parton distributions, while for $|x| < \xi$ the GPDs behave like meson distribution amplitudes.

The recent strong interest in GPDs was stimulated by the finding of Ji [2] that the second moment of the unpolarized GPDs at $\Delta^2 = 0$ is relevant to the spin structure

of the nucleon since it determines the total angular momentum of the quark flavor a:

$$J_a = \frac{1}{2}\int_{-1}^{+1} \mathrm{d}x x \left[H^a(x,\xi,\Delta^2=0) + E^a(x,\xi,\Delta^2=0)\right]. \tag{4}$$

A determination of contributions from all quark flavors gives the total quark angular momentum J_q which decomposes as

$$J_q = \frac{1}{2}\Delta\Sigma + L_q, \tag{5}$$

where $\Delta\Sigma/2$ and L_q denote quark spin and orbital angular momentum, respectively. As $\Delta\Sigma$ is measured through polarized DIS experiments, a measurement of J_q through (4) in terms of GPDs provides a model-independent way to determine the contribution of the quark orbital momentum to the nucleon spin. Eventually even the contribution of the total gluon angular momentum J_g may become accessible through

$$\frac{1}{2} = J_q + J_\mathrm{g}. \tag{6}$$

First measurements of the DVCS lepton helicity asymmetry have been accomplished recently by HERMES [9] at 27.5 GeV and by CLAS [10] at 4.25 GeV. Several plans exist for further measurements of DVCS and of other hard exclusive reactions to reach a first insight into GPDs. The DVCS process has also been observed in e^+p collider experiments at DESY by ZEUS [12] and H1 [13]. The DVCS cross-section was measured and compared to the QCD-based predictions. Measurements of the lepton beam helicity asymmetry by H1 and ZEUS will become possible in the near future when longitudinally polarized leptons will be made available also to the collider experiments at HERA.

The main aim of this paper is the evaluation of the anticipated statistical accuracy for future measurements of DVCS asymmetries. The kinematics and acceptance of the HERMES spectrometer, once upgraded with a recoil detector [11] for improved separation of exclusive events, was adopted to arrive at realistic numbers. In Sect. 2 of this paper different versions of GPD parameterizations are discussed. Section 3 deals with the assessment of the expected size of the asymmetries, based upon different GPD parameterizations, and with the evaluation of their projected statistical accuracy. Finally, in Sect. 4 the conclusions of this paper are presented.

2 Parameterization of generalized parton distributions

Two examples of GPD calculations are presently known in the literature. While bag model calculations [14] show a weak dependence of the distributions on the skewedness parameter, chiral quark soliton model calculations [15,16], in contrast, show a strong dependence on ξ. The common approach at the moment is to use a guess that satisfies general constraints on GPDs known from theory. This paper basically follows the ansatz proposed in [17,8]. Here, the dependence of the GPDs on Δ^2 is taken in a factorized form with respect to the other variables whereby satisfying (2). Any scale dependence of the GPDs is neglected.

In the simplest approach GPDs can be assumed to be independent of the skewedness parameter ξ. In the following, only u- and d-quark GPDs are considered to be non-zero. The function H, for example, is written as a product of an ordinary quark distribution function and a form factor,

$$\begin{aligned} H^u(x,\xi,\Delta^2) &= u(x)F_1^u(\Delta^2)/2, \\ H^d(x,\xi,\Delta^2) &= d(x)F_1^d(\Delta^2). \end{aligned} \tag{7}$$

Here $u(x)$ and $d(x)$ are the unpolarized quark distributions and $F_1^{u(d)}(\Delta^2)$ are defined through the electromagnetic form factors of proton and neutron:

$$F_1^u = 2F_1^p + F_1^n, \quad F_1^d = F_1^p + 2F_1^n. \tag{8}$$

In the same context, the function $\widetilde{H}$ is written in relation to quark helicity distributions and axial-vector form factors:

$$\begin{aligned} \widetilde{H}^u(x,\xi,\Delta^2) &= \Delta u_V(x) g_A^u(\Delta^2)/g_A^u(0), \\ \widetilde{H}^d(x,\xi,\Delta^2) &= \Delta d_V(x) g_A^d(\Delta^2)/g_A^d(0), \end{aligned} \tag{9}$$

where $g_A^u = (1/2)g_A + (1/2)g_A^0$, $g_A^d = -(1/2)g_A + (1/2)g_A^0$ and $g_A^0 = (3/5)g_A$.

The functions E and $\widetilde{E}$ have no definite limit at $\Delta^2 \to 0$, $\xi \to 0$, as it exists for the functions H and $\widetilde{H}$ (cf. (1)). In absence of any other guide the ansatz for E is chosen in a form analogous to the function H:

$$\begin{aligned} E^u(x,\xi,\Delta^2) &= u(x)F_2^u(\Delta^2)/2, \\ E^d(x,\xi,\Delta^2) &= d(x)F_2^d(\Delta^2), \end{aligned} \tag{10}$$

where $F_2^{u(d)}$ is defined in the same way as $F_1^{u(d)}$ in (8).

The function $\widetilde{E}$ is modeled to be due to the pion pole [16]:

$$\begin{aligned} \widetilde{E}^u(x,\xi,\Delta^2) &= -\widetilde{E}^d(x,\xi,\Delta^2) \\ &= \frac{1}{2}\widetilde{E}_{\pi\,\mathrm{pole}}(x,\xi,\Delta^2), \end{aligned} \tag{11}$$

$$\widetilde{E}_{\pi\,\mathrm{pole}}(x,\xi,\Delta^2) = \theta\left(-\xi \le x \le \xi\right) h_A(\Delta^2)\frac{1}{\xi}\Phi\left(\frac{x}{\xi}\right), \tag{12}$$

where $\Phi(z) = 3/4(1-z^2)$ is the pion distribution amplitude, $h_A(\Delta^2) = (4M^2 g_A)/(m_\pi^2 - \Delta^2)$, and $\theta(x)$ is the usual step function.

To introduce, as a next step, a dependence of the GPDs on the skewedness parameter ξ, the double-distribution formalism [1,3] can be used. In this model, the Δ^2-independent part of the function H can be written in the following form:

$$H^q_{\mathrm{DD}}(x,\xi) = \int_{-1}^{1}\mathrm{d}y \int_{-1+|y|}^{1-|y|}\mathrm{d}t\,\delta(x-y-t\xi)h(y,t)q(y). \tag{13}$$

Here $q(y)$ is the ordinary quark distribution and $h(y,t)$ is the so-called profile function:

$$h(y,t) = \frac{\Gamma(2b+2)}{2^{2b+1}\Gamma^2(b+1)} \frac{[(1-|y|)^2 - t^2]^b}{(1-|y|)^{2b+1}}, \qquad (14)$$

with b a free parameter and $b \to \infty$ corresponding to the skewedness-independent parameterization. Analogous expressions can be written for the functions $\widetilde{H}$ and E.

The functions H and E in the form of double distributions lack the correct polynomiality properties of GPDs. However, they can be restored by introducing the so-called D-term [18]. The D-term contribution has a different sign for H and E and hence is canceled in Ji's angular momentum relation, (4). The full model expressions for the GPDs therefore have the following form:

$$H^q(x,\xi) = H^q_{\rm DD}(x,\xi) + \theta(\xi - |x|)\frac{1}{N_f} D\left(\frac{x}{\xi}\right),$$
$$E^q(x,\xi) = E^q_{\rm DD}(x,\xi) - \theta(\xi - |x|)\frac{1}{N_f} D\left(\frac{x}{\xi}\right), \qquad (15)$$

where $N_f = 3$ is the number of active flavors. The parameterization of the D-term is taken in a form that follows from chiral quark soliton model calculations [19]. For more details on possible GPD parameterizations and their discussion we refer to [17,8].

Quark number density and quark helicity distributions $q(x)$ and $\Delta q(x)$, respectively, were used in the parameterizations of [20] (at $Q^2 = 2\,\mathrm{GeV}^2$) and [21] (at $Q^2 = 1\,\mathrm{GeV}^2$).

In the projections described below five different versions of GPD parameterizations were included:

(A) $H(x,\xi)$, $\widetilde{H}(x,\xi)$, and $E(x,\xi)$ are skewedness independent and given by (7), (9), and (10), respectively.
(B) The skewedness dependence of $H(x,\xi)$, $\widetilde{H}(x,\xi)$, and $E(x,\xi)$ is generated through the double-distribution formalism (13) and (14) with the parameter $b = 1$.
(C) Same as (B), but with the parameter $b = 3$.
(D) Same as (B), but the contribution of the D-term to $H(x,\xi)$ and $E(x,\xi)$ is included additionally, according to (15).
(E) Same as (D), but with the parameter $b = 3$.

For $\widetilde{E}(x,\xi)$ the pion pole expression (11) is used for all versions of GPDs.

The dependences of the GPDs on the variables x and ξ (at $\Delta^2 = 0$), obtained from these five different parameterizations, are displayed for a few examples in Fig. 1. Panels (a) and (b) show the GPD H in version (B) for different values of ξ, compared between u- and d-quark. Panels (c) and (d) show the unpolarized u-quark GPDs H and E at fixed $\xi = 0.4$, compared between different versions: (B) as a solid line, (C) as a dashed line and (D) as a dotted line. Panels (e) and (f) show the polarized u-quark GPDs $\widetilde{H}$ and $\widetilde{E}$ in version (B) compared for different values of ξ. Although $\widetilde{E}$ does not appear in the DVCS asymmetries (see below), its u- versus d-quark comparison is shown as well. By definition $\widetilde{E}$ is large at $\Delta^2 = 0$ (see (11)).

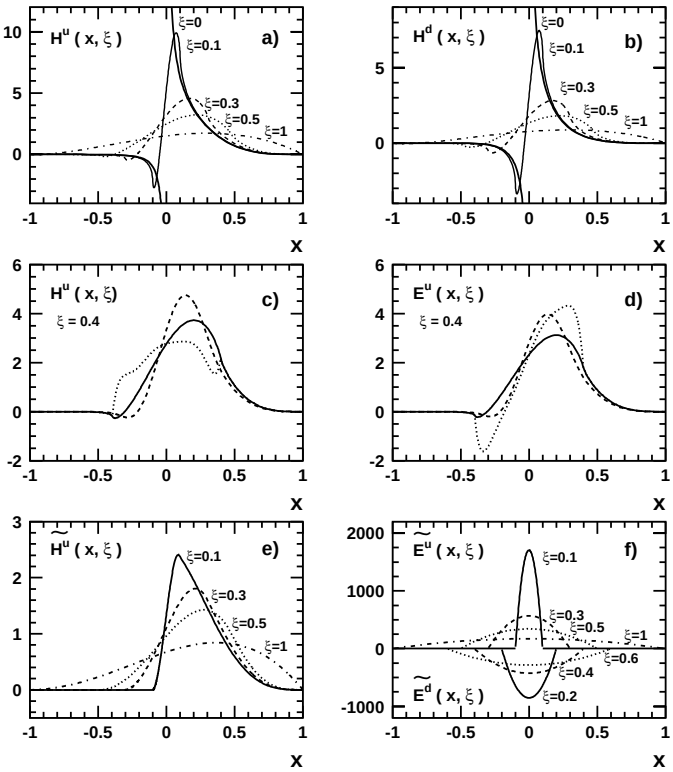

Fig. 1a–f. Illustration of the x-behavior of various generalized parton distributions for different values of the skewedness parameter ξ (at $\Delta^2 = 0$). For explanation see text

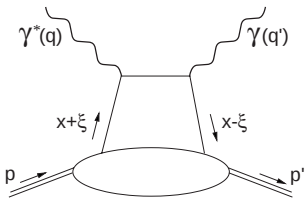

Fig. 2. Leading handbag diagram for DVCS

3 Deeply virtual Compton scattering

In the Bjorken limit, DVCS is dominated by the handbag diagram (Fig. 2) and its amplitude can be factorized into a soft part described by GPDs and a hard part representing a parton process calculable in perturbative QCD. In this limit the skewedness parameter ξ can be related to the Bjorken variable $x_{\rm B}$:

$$\xi = \frac{x_{\rm B}/2}{1 - x_{\rm B}/2}. \qquad (16)$$

The same final state, $ep\gamma$, can also be produced via the Bethe–Heitler (BH) process in which an electron scatters elastically off the target proton and the initial or final state electron radiates a real photon. The cross-section of this process can be calculated exactly once the Dirac and Pauli nucleon form factors are known. On the one hand, the BH process constitutes the main background to DVCS, on the other hand their interference opens the unique opportunity for independent measurements of the

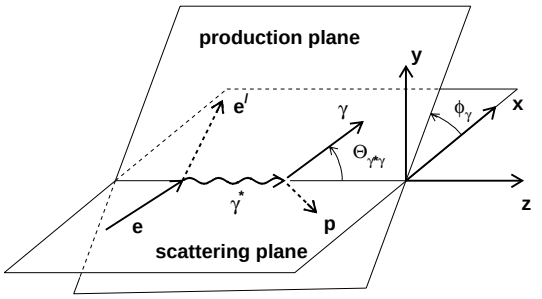

Fig. 3. Kinematic configuration for the process $ep \longrightarrow ep\gamma$

real and imaginary parts of a certain DVCS amplitude combination (see below).

The cross-section of the DVCS process and its interference with the BH process has been considered in a number of papers [2,3]. The kinematic configuration of the process $ep \longrightarrow ep\gamma$ is shown in Fig. 3. Here ϕ_γ describes the azimuthal orientation of the production plane (comprising γ^*, γ and p) relative to the scattering plane (comprising the initial and final lepton, as well as the virtual photon). The laboratory polar angle between virtual and real photon is denoted by $\theta_{\gamma\gamma^*}$. In-plane (i.e. $\phi_\gamma = 0$) differential cross-sections for DVCS, BH and total γ production in e^+p interactions at $E_e = 27.5\,\mathrm{GeV}$ were calculated following [2] and are presented in Fig. 4. The DVCS cross-section shows a maximum at $\Theta_{\gamma\gamma^*} = 0$, while the BH cross-section has a three-pole structure due to the propagators of the virtual electrons and the virtual photon. Although at this energy the cross-section of DVCS is smaller than that of BH over practically the entire kinematic region, the interference between both processes opens the possibility to access DVCS amplitudes [22,23].

In [24] amplitudes of DVCS, BH and of the interference terms were calculated at the leading twist-2 level for polarized and unpolarized initial particles. This approach was used to calculate projections for future measurements of DVCS–BH interference effects. For a first application the kinematics and acceptance of the HERMES experiment were chosen. In the context of the planned recoil detector upgrade the primary interest lies with measurements using an unpolarized proton target. In this case two different types of experiments are possible that will be giving insight into GPDs:

(I) Measurements of the lepton charge asymmetry with unpolarized leptons of either charge:

$$\mathrm{d}\Delta\sigma_{\mathrm{ch}} \equiv \mathrm{d}\sigma(e^+p) - \mathrm{d}\sigma(e^-p) \sim \cos(\phi_\gamma) \times \mathrm{Re}\left\{F_1\mathcal{H}_1 + \frac{x_\mathrm{B}}{2-x_\mathrm{B}}(F_1+F_2)\widetilde{\mathcal{H}}_1 - \frac{\Delta^2}{4M^2}F_2\mathcal{E}_1\right\}. \quad (17)$$

This asymmetry allows one to have access to the real parts of the DVCS amplitudes $\mathcal{H}_1$, $\widetilde{\mathcal{H}}_1$, and $\mathcal{E}_1$.

(II) Measurements of the beam helicity asymmetry using a polarized positron beam:

$$\mathrm{d}\Delta\sigma_{LU} \equiv \mathrm{d}\sigma(\overrightarrow{e^+}p) - \mathrm{d}\sigma(\overleftarrow{e^+}p) \sim \sin(\phi_\gamma) \times \mathrm{Im}\left\{F_1\mathcal{H}_1 + \frac{x_\mathrm{B}}{2-x_\mathrm{B}}(F_1+F_2)\widetilde{\mathcal{H}}_1 - \frac{\Delta^2}{4M^2}F_2\mathcal{E}_1\right\}. \quad (18)$$

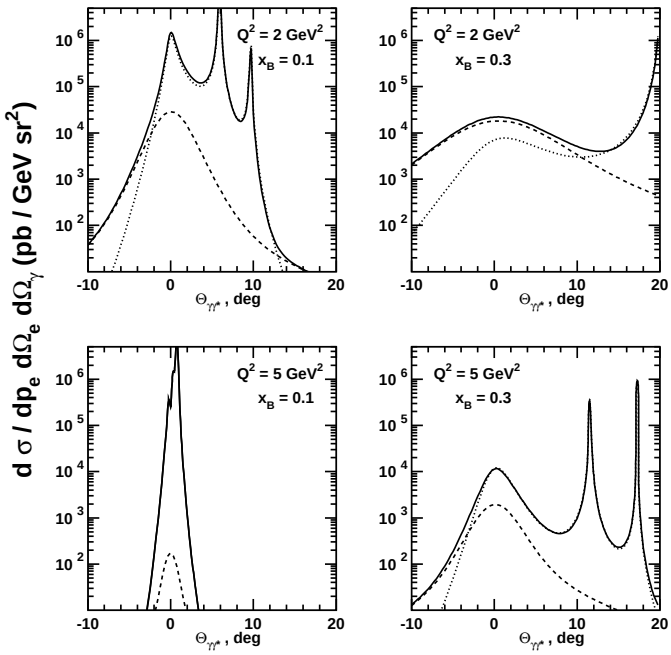

Fig. 4. Illustration of the behavior of the differential in-plane cross-section as a function of the polar angle between the virtual and the real photon for DVCS (dashed lines), Bethe–Heitler (dotted lines) and total γ production (solid lines) in e^+p interactions at HERMES energy $E_e = 27.5\,\mathrm{GeV}$. Different panels are for different values of x_B and Q^2

This asymmetry allows one to have access to the imaginary parts of the same amplitudes.

The imaginary and real parts of the DVCS amplitudes $\mathcal{H}_1$ and $\widetilde{\mathcal{H}}_1$ are related to the GPDs H and $\widetilde{H}$ as follows:

$$\begin{aligned}
&\mathrm{Im}\mathcal{H}_1 = -\pi\sum_q e_q^2(H^q(\xi,\xi,\Delta^2) - H^q(-\xi,\xi,\Delta^2)),\\
&\mathrm{Im}\widetilde{\mathcal{H}}_1 = -\pi\sum_q e_q^2(\widetilde{H}^q(\xi,\xi,\Delta^2) + \widetilde{H}^q(-\xi,\xi,\Delta^2)),\\
&\mathrm{Re}\mathcal{H}_1\\
&= \sum_q e_q^2\left[P\int_{-1}^{+1} H^q(x,\xi,\Delta^2)\left(\frac{1}{x-\xi}+\frac{1}{x+\xi}\right)\mathrm{d}x\right],\\
&\mathrm{Re}\widetilde{\mathcal{H}}_1 \qquad (19)\\
&= \sum_q e_q^2\left[P\int_{-1}^{+1} \widetilde{H}^q(x,\xi,\Delta^2)\left(\frac{1}{x-\xi}-\frac{1}{x+\xi}\right)\mathrm{d}x\right],
\end{aligned}$$

where P denotes Cauchy's principal value. The DVCS amplitudes $\mathcal{E}_1$ and $\widetilde{\mathcal{E}}_1$ can be expressed through E and $\widetilde{E}$ analogously.

Projections for statistical accuracies attainable in measurements of the lepton charge and lepton beam helicity asymmetry were calculated in the HERMES kinematics for an anticipated integrated luminosity of $2\,\mathrm{fb}^{-1}$ [11] which corresponds to the expected value for one year of data taking. The HERMES geometrical acceptance for the detection of the scattered electron, the photon and the recoil proton was taken into account. The following kine-

matic cuts[1] were applied: $E_e > 3.5\,\mathrm{GeV}$, $W^2 > 4\,\mathrm{GeV}^2$, $Q^2 > 1\,\mathrm{GeV}^2$, $E_\gamma > 1\,\mathrm{GeV}$, $P_p > 0.2\,\mathrm{GeV}$, $0.35 < \theta_p^{\mathrm{lab}} < 1.35\,\mathrm{rad}$, and $15 < \Theta_{\gamma\gamma^*} < 70\,\mathrm{mrad}$. Note that the last cut corresponds to a narrow region in the center of the plots shown in Fig. 4.

To calculate the asymmetries (17) and (18) the 5-fold differential cross-section has to be integrated over the appropriate kinematic region accounting for the geometrical acceptance:

$$\frac{\mathrm{d}\sigma}{\mathrm{d}\phi_\gamma} = \int \frac{\mathrm{d}^5\sigma}{\mathrm{d}x_B \mathrm{d}Q^2 \mathrm{d}|\Delta^2| \mathrm{d}\phi_\gamma \mathrm{d}\phi_{\mathrm{el}}} \mathrm{d}x_B \mathrm{d}Q^2 \mathrm{d}|\Delta^2| \mathrm{d}\phi_\gamma \mathrm{d}\phi_{\mathrm{el}},$$

where ϕ_{el} is the azimuthal angle of the scattered electron. It is appropriate to define differences and sums of certain cross-sections:

$$\begin{aligned}
\frac{\mathrm{d}\Delta\sigma_{\mathrm{ch}}}{\mathrm{d}\phi_\gamma} &= \frac{\mathrm{d}\sigma(e^+p)}{\mathrm{d}\phi_\gamma} - \frac{\mathrm{d}\sigma(e^-p)}{\mathrm{d}\phi_\gamma}, \\
\frac{\mathrm{d}\Sigma\sigma_{\mathrm{ch}}}{\mathrm{d}\phi_\gamma} &= \frac{\mathrm{d}\sigma(e^+p)}{\mathrm{d}\phi_\gamma} + \frac{\mathrm{d}\sigma(e^-p)}{\mathrm{d}\phi_\gamma}, \\
\frac{\mathrm{d}\Delta\sigma_{LU}}{\mathrm{d}\phi_\gamma} &= \frac{\mathrm{d}\sigma(e^\uparrow p)}{\mathrm{d}\phi_\gamma} - \frac{\mathrm{d}\sigma(e^\downarrow p)}{\mathrm{d}\phi_\gamma}, \\
\frac{\mathrm{d}\Sigma\sigma_{LU}}{\mathrm{d}\phi_\gamma} &= \frac{\mathrm{d}\sigma(e^\uparrow p)}{\mathrm{d}\phi_\gamma} + \frac{\mathrm{d}\sigma(e^\downarrow p)}{\mathrm{d}\phi_\gamma}.
\end{aligned} \tag{20}$$

Using these definitions the ϕ-dependence of the lepton charge asymmetry reads

$$A_{\mathrm{ch}}(\phi) = \frac{\int_{\phi-\Delta\phi}^{\phi+\Delta\phi} \mathrm{d}\phi \mathrm{d}\Delta\sigma_{\mathrm{ch}}/\mathrm{d}\phi}{\int_{\phi-\Delta\phi}^{\phi+\Delta\phi} \mathrm{d}\phi \mathrm{d}\Sigma\sigma_{\mathrm{ch}}/\mathrm{d}\phi}, \tag{21}$$

while an integrated lepton charge asymmetry can be defined by forming the difference between two integrals over appropriately defined "halves" of the ϕ-distribution:

$$\widetilde{A}_{\mathrm{ch}} = \frac{\int_{-\pi/2}^{\pi/2} \mathrm{d}\phi \mathrm{d}\Delta\sigma_{\mathrm{ch}}/\mathrm{d}\phi - \int_{\pi/2}^{3\pi/2} \mathrm{d}\phi \mathrm{d}\Delta\sigma_{\mathrm{ch}}/\mathrm{d}\phi}{\int_0^{2\pi} \mathrm{d}\phi \mathrm{d}\Sigma\sigma_{\mathrm{ch}}/\mathrm{d}\phi}. \tag{22}$$

Analogously the ϕ-dependent and the integrated lepton beam helicity asymmetry, respectively, are defined as follows:

$$A_{LU}(\phi) = \frac{\int_{\phi-\Delta\phi}^{\phi+\Delta\phi} \mathrm{d}\phi \mathrm{d}\Delta\sigma_{LU}/\mathrm{d}\phi}{\int_{\phi-\Delta\phi}^{\phi+\Delta\phi} \mathrm{d}\phi \mathrm{d}\Sigma\sigma_{LU}/\mathrm{d}\phi}, \tag{23}$$

$$\widetilde{A}_{LU} = \frac{\int_0^{\pi} \mathrm{d}\phi \mathrm{d}\Delta\sigma_{LU}/\mathrm{d}\phi - \int_{\pi}^{2\pi} \mathrm{d}\phi \mathrm{d}\Delta\sigma_{LU}/\mathrm{d}\phi}{\int_0^{2\pi} \mathrm{d}\phi \mathrm{d}\Sigma\sigma_{LU}/\mathrm{d}\phi}. \tag{24}$$

Projections for the statistical accuracy attainable in measuring the lepton charge asymmetry are presented in Fig. 5. The results are shown as a function of the azimuthal angle ϕ_γ in two regions of x_{B}, using different GPD parameterizations. The asymmetry clearly depends on the particular parameterization and can even change its sign in dependence on x_B. Therefore, in the experiment the asymmetry will have to be studied differentially as much as possible. Apparently, the inclusion of the D-term leads to essential changes in the asymmetry and future measurements may allow one to confirm its importance experimentally. In Fig. 6 the integrated lepton charge asymmetry $\widetilde{A}_{\mathrm{ch}}$ is shown as a function of x_{B} and Δ^2, based on the GPD parameterization (E). No Δ^2-dependence is seen on the basis of the chosen GPD model.

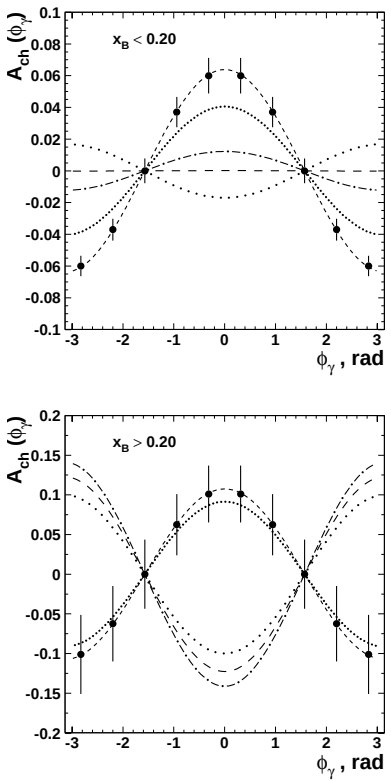

Fig. 5. Projected statistical accuracy for the lepton charge asymmetry (21) as a function of the azimuthal angle ϕ_γ between scattering plane and production plane. Predictions of different GPDs models (see text) are shown in two regions of x_{B}. Version (A) is denoted by a dash-dotted line; version (B) by a long-space dotted line; version (C) by a long-space dashed line; version (D) by a dotted line; version (E) by a dashed line

Projections for the statistical accuracy attainable in measurements of the helicity asymmetry are presented in Fig. 7, as a function of the azimuthal angle ϕ_γ (top panel) and as a function of x_{B} and Δ^2 (bottom panel). As can be seen, the projections of the statistical accuracy promise a considerable improvement compared to the present HERMES measurement [9] shown additionally in Fig. 7 (top panel). The projected asymmetry changes only slightly in dependence on the GPD parameterizations when the parameter b of the profile function (14) varies in the range $(1, \infty)$. Note that the beam helicity asymmetry is not sen-

[1] Here E_e and E_γ are the energy of the incoming electron and the outgoing photon, respectively, while P_p is the momentum of the outgoing proton. The standard DIS variables Q^2 and W describe the negative four-momentum transfer squared and the energy of the $\gamma^* p$ system, respectively. The laboratory polar angle of the outgoing proton is given by θ_p^{lab}

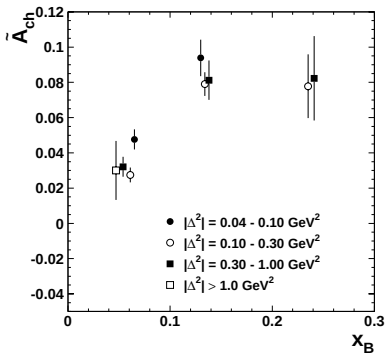

Fig. 6. Projected statistical accuracy for the ϕ-integrated lepton charge asymmetry (22) as a function of x_B and Δ^2 based upon GPD model version (E)

sitive to the D-term as it does not contribute to the imaginary parts of DVCS amplitudes.

The considerations presented above are based upon the leading twist-2 level using the amplitudes calculated in [24]. More elaborate approaches may include twist-3 effects [19,25] and next-to-leading order calculations [26, 27]. These calculations show that the corrections to leading order can be quite large. Nevertheless, in the present situation, where the generalized parton distributions are practically unknown, the approach adopted in this paper appears adequate to evaluate the size of the asymmetries expected in future measurements.

It appears worth noting that important results on GPDs can be expected from the analysis of the same data set by studying hard exclusive production of both pseudoscalar and vector mesons. As compared to DVCS these processes will provide information on different combinations of generalized parton distributions.

4 Conclusions

Expected statistical accuracies have been evaluated for future measurements of deeply virtual Compton scattering. Kinematics and acceptance of the HERMES spectrometer, complemented with a recoil detector, have been adopted for the calculations presented in this paper. Using polarized electrons and positrons of HERA with different helicities, in conjunction with an unpolarized proton target, it becomes possible to measure the lepton charge asymmetry and the lepton beam helicity asymmetry, both induced by the interference of the DVCS and the Bethe–Heitler process. From these asymmetries the real and the imaginary part of a certain DVCS amplitude combination can be determined.

The expected size of the asymmetries has been evaluated using various parameterizations of the underlying generalized parton distributions. A number of different parameterizations has been used to compensate as much as possible for the present poor knowledge on GPDs. The level of the attainable statistical accuracy is mainly determined by the cross-section of the Bethe–Heitler process

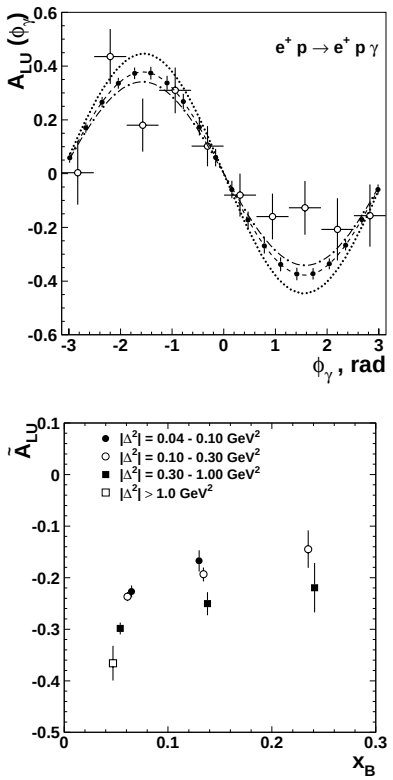

Fig. 7. Projected statistical accuracy for the beam helicity asymmetry (23) and (24) as a function of the azimuthal angle ϕ_γ between scattering plane and production plane (top panel, closed circles) and as a function of x_B and Δ^2 (bottom panel). The line conventions are as in Fig. 5. The present measurement of the azimuthal asymmetry by HERMES [9] is shown in the top panel by open circles

that dominates the reaction $ep \to ep\gamma$ at the given energy.

It has been shown that measurements of hard exclusive real photon production at HERMES will be of high statistical significance. The envisaged separate results on the real and the imaginary part of a certain DVCS amplitude combination will constitute an important step towards the determination of the generalized parton distributions. The measured constraints will serve as very useful input for the further modeling of generalized parton distributions. Nevertheless, for a successful extraction of GPDs from experimental observables further theoretical work is required. An actual list of problems that need further investigation has recently been given in [8].

Acknowledgements. We are indebted to J. Blümlein and M. Diehl for valuable comments and to R. Kaiser for careful reading of the manuscript.

References

1. D. Müller et al., Fortsch. Phys. **42**, 101 (1994)
2. X. Ji, Phys. Rev. Lett. **78**, 610 (1997); Phys. Rev. D **55**, 7114 (1997)

3. A.V. Radyushkin, Phys. Lett. B **380**, 417 (1996); Phys. Rev. D **56**, 5524 (1997)
4. J. Blümlein, B. Geyer, D. Robaschik, Phys. Lett. B **406**, 161 (1997); Nucl. Phys. B **560**, 283 (1999); I. Balitsky, A.V. Radyushkin, Phys. Lett. B **413**, 114 (1997)
5. J. Blümlein, D. Robaschik, Nucl. Phys. B **581**, 449 (2000)
6. J. Blümlein et al., DESY-01-108, hep-ph/0108095
7. A.V. Radyushkin, hep-ph/0101225
8. K. Goeke, M.V. Polyakov, M. Vanderhaeghen, Prog. Part. Nucl. Phys. **47**, 401 (2001); hep-ph/0106012
9. A. Airapetian et al., Phys. Rev. Lett. **87**, 182001 (2001)
10. S. Stepanyan et al., Phys. Rev. Lett. **87**, 182002 (2001)
11. A Large Acceptance Recoil Detector for HERMES, DESY PRC 01-01, April 2001
12. P.R.B. Saull, Proceedings of the International Europhysics Conference on HEP, Tampere, Finland, 15–21 July 1999, edited by K. Huitu, H. Kurki-Suonio, J. Maalampi (hep-ex/0003030); L. Favart, DIS-2001, Bologna, 27 April–1 May (hep-ex/0106067)
13. C. Adloff et al., Phys. Lett. B **517**, 47 (2001)
14. X. Ji, W. Melnitchouk, X. Song, Phys. Rev. D **56**, 5511 (1997)
15. V. Petrov et al., Phys. Rev. D **57**, 4325 (1998)
16. M. Penttinen, M.V. Polyakov, K. Goeke, Phys. Rev. D **62**, 014024 (2000)
17. M. Vanderhaeghen, P.A.M. Guichon, M. Guidal, Phys. Rev. D **60**, 094017 (1999)
18. M.V. Polyakov, C. Weiss, Phys. Rev. D **60**, 114017 (1999)
19. N. Kivel, M.V. Polyakov, M. Vanderhaeghen, Phys. Rev. D **63**, 114014 (2001)
20. A.D. Martin et al., Eur. Phys. J. C **4**, 463 (1998)
21. E. Leader, A.V. Sidorov, D.B. Stamenov, Phys. Rev. D **58**, 114028 (1998)
22. M. Diehl et al., Phys. Lett. B **411**, 193 (1997)
23. L.L. Frankfurt, A. Freund, M. Strikman, Phys. Rev. D **58**, 114001 (1998)
24. A.V. Belitsky et al., Nucl. Phys. B **593**, 289 (2001)
25. A.V. Belitsky et al., Phys. Lett. B **510**, 117 (2001)
26. A.V. Belitsky et al., Phys. Lett. B **474**, 163 (2000)
27. A. Freund, M. McDermott, hep-ph/0106124